Spatial photosynthesis modelling sets guidelines to constructing a viable single-cell cytoplasm-to-stroma C_4 cycle

Ivan Jurić[a,*], Julian M. Hibberd[b], Mike Blatt[c], Nigel J. Burroughs[a,*]

[a]*Warwick Systems Biology Centre, University of Warwick, Coventry, CV4 7AL, UK*
[b]*Department of Plant Sciences, University of Cambridge, Cambridge, CB2 3EA, UK*
[c]*Institute of Molecular Cell and Systems Biology, University of Glasgow, Glasgow, G12 8QQ, UK*

Abstract

It has been proposed that introducing C_4 photosynthesis into C_3 crops would increase yield. The simplest scheme involves concentrating carbon originating from the cytosol in the chloroplast stroma of mesophyll cells without altering leaf or cell anatomy. Photosynthetic efficiency would then strongly depend on the chloroplast envelope permeability to CO_2. We examine the performance of this C_4 cycle with a spatial model of carbon assimilation in C_3 mesophyll cell geometry, conducting a thorough exploration of parameter space relevant to C_4 photosynthesis. For envelope permeabilities below $300\,\mu$m/s C_4 photosynthesis has a higher quantum efficiency than C_3. However, even when envelope permeability is above this threshold, the C_4 pathway can provide a substantial boost to carbon assimilation with only a moderate decrease in efficiency. Depending on the available light-harvesting capacity of plastids, C_4 photosynthesis could boost carbon assimilation anywhere from 20% to 100%. Gains are even more prominent under CO_2 deprivation, and can be achieved in conjunction with lower investment in plastids if chloroplast surface coverage is also altered. A C_4 pathway operating within individual mesophyll cells of C_3 plants could hence lead to higher growth rates and better drought resistance in dry, high-sunlight climates.

Introduction

Various strategies have been proposed to introduce a C_4 cycle into C_3 crops with the aim of boosting productivity (Furbank et al., 2013). The evolution of C_4 photosynthesis is commonly associated with multiple modifications to leaf anatomy, cell biology, and the biochemistry of photosynthesis. Thus, even with rapid advances in our ability to modify plant biology, the endeavour to re-engineer C_4 photosynthesis is considered challenging. Innovative and versatile theoretical models are therefore needed to guide the design and implementation of carbon concentrating mechanisms in C3 species.

C_4 photosynthesis is a biochemical carbon-concentrating pump that has evolved over sixty times in higher plants (Sage, 2004). It typically appears in conjunction with so-called Kranz anatomy in which concentric layers of bundle

---

[*]Corresponding authors. Emails: i.juric@warwick.ac.uk, n.j.burroughs@warwick.ac.uk.

sheath and then mesophyll cells cooperate in the photosynthetic process. Photosynthesis in C_4 plants is therefore associated with multiple cell walls acting as diffusion barriers to CO_2 (Sage, 2004). In a small number of species, the C_4 cycle is contained within individual mesophyll cells (von Caemmerer et al., 2014). It is thought that spatial separation between the primary and the secondary carboxylases (PEPC and RubisCO) in enlarged mesophyll cells phenocopies the diffusion barriers found in two-celled C_4 plants (von Caemmerer et al., 2014). Introducing a single-cell C_4 cycle in C_3 organisms is appealing as the substantial anatomical remodelling of C_4 leaves and cellular architecture associated with Kranz anatomy could be avoided. However, single-cell C_4 plants also feature notable modifications to the architecture of mesophyll cells, which facilitate the larger spatial separation (von Caemmerer et al., 2014).

Spatial separation between PEPC and RubisCO aids the C_4 pump by providing increased diffusive resistance and essentially underpins single-cell C_4 efficacy (Jurić et al., 2017). However, it is not clear if such cell-scale spatial separation is strictly necessary. To investigate this, we develop a spatial model of a minimal C_4 pathway operating in an unaltered C_3 mesophyll cell geometry. The pathway would draw carbon from the cytoplasm and concentrate it within the chloroplast stroma. It would require targeted expression of the pathway enzymes in the cytoplasm and the stroma, a change in the expression of transporters in the chloroplast envelope to transport C_3 and C_4 acids, and a C_4 regulatory mechanism to switch it off when energy/reductant availability is low.

This minimal C_4 photosynthetic system has previously been discussed by von Caemmerer and Furbank (von Caemmerer and Furbank, 2003; von Caemmerer, 2003) who modelled it within a compartmental paradigm. Their conclusions suggested that although a C_4 cycle could result in higher CO_2 assimilation rates, this would come at the expense of a substantially lower energetic efficiency of photosynthesis. However, their analysis assumed a relatively high conductance of the chloroplast envelope, the cell wall, and the plasmalemma (see Discussion). Due to a small spatial separation ($\sim 1\,\mu$m) between the carboxylase and decarboxylase of the proposed C_4 pump (which is well below the threshold separation ($\sim 10\,\mu$m) for cost efficient single-cell C_4 photosynthesis (Jurić et al., 2017)) the viability of a single-cell based system would be strongly influenced by the permeability of the chloroplast envelope since this determines the CO_2 leakage current.

CO_2 permeabilities of biological barriers are uncertain, with estimates of chloroplast envelope permeability ranging over three orders of magnitude, $10^1 - 10^4\,\mu$m/s (Evans et al., 2009; Kaldenhoff et al., 2014). We deal with the issue of important input parameters that are poorly characterised by modelling C_4 photosynthesis for the entire range of reported values. Even so, in order to determine if the proposed C_4 cycle is viable, we need a criterion to decide whether a particular choice of parameter values is reasonable. One straightforward and simple criterion is that the parameter choice can replicate the known quantum efficiency of regular C_3 photosynthesis in its native geometry ($\gtrsim 0.05$, or equivalently a photon cost ≈ 20/C (Ehleringer and Pearcy, 1983)). We also quantify the ability of a plastid to absorb and utilise photons for carbon assimilation, by requiring that it does not limit C_3 photosynthesis under normal conditions. This *light-harvesting capacity* is important because it may constrain assimilation of the proposed C_4 system and limit attainable yields. We examine the physical parameters affecting C_3 photosynthetic efficiency in greater detail in a separate publication (under review).

2

The model we use is based on one previously constructed to study single-cell C_4 photosynthesis in Bienertia (Jurić et al., 2017). It focuses on the effect of intracellular geometry on the diffusive transport of photosynthetically relevant gasses (O_2, CO_2, and its hydrated form HCO_3^-). The diffusion of these species is commonly a limiting factor for both C_3 and C_4 photosynthesis. Photochemistry and metabolism (light capture, ATP/NADPH production, Calvin cycle, and photorespiration) are assumed to function optimally. The model is similar in some aspects to the 3D model of C_3 photosynthesis presented in Tholen and Zhu (2011) but there are notable differences. Most importantly, we include C_4 biochemistry, but we also explicitly treat oxygen's kinetics and diffusion, whilst utilising the system's symmetry to reduce the computational burden, permitting a thorough investigation of the parameter space. By examining how photosynthesis is affected by variation in cell geometry or biochemistry, we can determine when the C_4 cycle is viable and what alterations are needed to make it a beneficial addition.

The photosynthesis model

The following is a brief outline of the model. Additional details are provided in the Supplementary Material.

Geometry

A typical C_3 mesophyll cell has one large central vacuole that occupies the majority of the cell volume with other organelles located around the cell's periphery. Chloroplasts in particular, press against the cell membrane in regions adjacent to the intercellular airspace (IAS). Their density is high, with around 50%-70% of the cell surface covered by plastids in a roughly hexagonal lattice arrangement (Figure 1(b)) (Ellis and Leech, 1985; Tholen et al., 2008). Much smaller mitochondria can move freely within the peripheral cytoplasm, which we model as a single homogeneous photorespiring compartment.

Since both sources and sinks for CO_2 are located at the cell's periphery, we expect the vacuole space, especially deeper in the cell interior, to play only a minor role in transport of O_2 and CO_2. We therefore focus on a single, typical peripheral plastid and its immediate environment (the spatial region closer to this plastid than to its neighbours), simplifying this approximately hexagonal region as a cylinder (Figure 1(a,b)) that contains one axially-centred semi-spherical plastid. The radius of the cylinder determines the chloroplast surface coverage fraction.

Transport and biochemistry

We focus on three inorganic species - O_2, CO_2, and HCO_3^- - solving for their position-dependent steady-state concentration profiles in order to derive photosynthetic currents. Other metabolites, such as RuBP or PEP, are constrained to the liquid phase and typically do not permeate inter-compartmental boundaries. Their operating pools can in principle be as large as required for optimal photosynthesis, so we assume their levels are not limiting. In contrast, O_2 and CO_2 are gasses and readily diffuse within and between cellular compartments, and between the mesophyll interior and outside air. Because of this gaseous exchange, the efficacy of both C_3 and C_4 photosynthesis is heavily dependent on their diffusion rates.

Diffusion of the modelled species within particular cellular compartments is quantified by the local viscosities, while diffusion across the inter-compartmental barriers is characterised by barrier permeabilities. Diffusing gasses can enter and exit the simulated region through one of the cylinder ends representing the inner surface of the cell membrane (Figure 1(a)).

Although HCO_3^- cannot diffuse through intracellular membranes, it too has to be treated explicitly as it strongly couples to the CO_2 pool in the chloroplast stroma and in the cytoplasm, where we assume CA is present. The CA-assisted interconversion between CO_2 and HCO_3^- is modelled as a boost to the base pH-dependent interconversion rates. This accounts for both the efficiency of CA and its concentration.

The reaction of HCO_3^- with the PEPC-bound PEP in the cytoplasm is the entry point of carbon in the C_4 cycle. The PEP carboxylation rate determines the rate of CO_2 release from C_4-acid decarboxylation in the stroma. The concentration of cytoplasmic PEPC will serve as a measure of C_4 pathway expression.

RubisCO-bound RuBP in the chloroplast stroma reacts with CO_2 and with O_2. The reactions are the key initial steps of the Calvin-Benson cycle and photorespiration. The RuBP oxygenation rate determines the rate of photorespiratory CO_2 release in the peripheral cytoplasm. The reductant (NADPH) consumption by the Calvin-Benson cycle and photorespiration must be matched by its production via the linear electron transfer chain. This couples O_2 production on the chloroplast thylakoid with RuBP carboxylation and oxygenation rates.

Energy input and measures

The assimilation, determined by the throughput of the photorespiratory and Calvin-Benson cycle pathways, is expressed on a cell-surface-area basis. The photon cost of carbon fixation (the number of photons needed per assimilated carbon atom to cover for the costs of the Calvin-Benson cycle, the photorespiration, and the C_4 cycle) is quantified assuming optimal usage of the linear and cyclic electron transfer chains (Zhu et al., 2008, 2010; Jurić et al., 2017). The total energy consumption is expressed in terms of (photosynthetically active) photons absorbed per stroma volume in unit time, as in Xiao et al. (2016). This consumption cannot exceed the light-harvesting capacity of plastids. As an illustrative reference, a photon consumption rate of 20 mM/s is equivalent to the absorption of 1% of the maximal photosynthetically active solar flux (2 mmol/m^{2}s (Björkman and Demmig-Adams, 1995)) that is perpendicularly incident on the parts of the cell surface covered by the plastids (assuming default plastid geometry parameters, Table 1).[1]

The limited light availability or light-harvesting capacity is modelled by scaling-down the concentrations of the substrate-primed enzymes involved in photosynthesis (i.e. RuBP-primed RubisCO and PEP-primed PEP-carboxylase), when energy requirements exceed the supply threshold. The adjustment reflects the limited substrate availability caused by energy scarcity.[2]

---

[1] At 50% plastid surface coverage, this corresponds to 0.5 % of maximal solar flux passing through the cell surface.

[2] The effective RubisCO and PEPC concentrations are scaled proportionally, so their carboxylating capacity ratio stays fixed. A plant with optimised control mechanisms could in principle independently alter the activity of the two carboxylases under light deprivation, but we do not assume the presence of such control mechanisms.

The choice of parameters

The default parameters for geometry and biochemistry in Table 1 correspond to *Triticum aestivum* (Ellis and Leech, 1985; Cousins et al., 2010), which we chose as a representative C_3 crop. Not all parameters are well known however, and some reflect environmental conditions. We therefore examine how the variation in potentially important physical parameters would affect the efficacy of the proposed C_4 pathway. This is executed by independently varying the selected parameter and the activity of the C_4 pump (i.e. the cytoplasmic PEPC level). Since the plastid envelope is expected to have a major influence on the efficiency of the pathway, we focus on varying its permeability, while keeping the combined permeability of the cell wall and plasmalemma at $\sigma_C = 200\,\mu$m/s (representing the mid-range of experimental estimates provided by Terashima et al. (2006) and Evans et al. (2009)). The permeability of the vacuole membrane always defaults to twice the envelope permeability (the latter being a double membrane). The actual effect of independently varying the vacuole membrane permeability will be shown to be negligible. The concentration of RubisCO active sites in the stroma is kept at 4 mM. This represents the concentration of activated and RuBP-primed RubisCO, and is roughly in the middle of the known range of RubisCO active site concentration (2-5 mM; von Caemmerer (2000)).

When evaluating the relative efficiency of the C_4 cycle, we use C_3 photosynthesis *with the same amount* of CA in the cytoplasm as the baseline for comparison. Since cytoplasmic CA already improves photosynthesis slightly (see Results), using the 'enhanced' C_3 photosynthesis as a baseline benchmark will produce more conservative estimates of gains when introducing a C_4 cycle.

Results

We first examine photosynthesis without any imposed light-harvesting cap, only observing at which PEPC concentration a particular energy consumption threshold is reached. Later we examine what happens when an actual light-utilisation cap is imposed.

The impact of cytoplasmic and stromal CA on photosynthesis

There needs to be sufficient CA in the cytoplasm to allow for a fast conversion of CO_2 into bicarbonate, which is a substrate for PEPC. CA is known to be present in the chloroplast stroma in C_3 plants (Tiwari et al., 2005; Tsuzuki et al., 1985). There is also some evidence of cytoplasmic CA expression (Tiwari et al., 2005; Fabre et al., 2007), although the level of its activity and its effect on photosynthesis remains unknown. It has been conjectured that the stromal CA's purpose is to boost CO_2 diffusion within the plastid, or to facilitate CO_2 transfer through the envelope by generating a larger CO_2 gradient across this diffusion barrier (Badger, 2003). Previous modelling has shown a minor positive impact on the assimilation rate attributable to stromal CA (Tholen and Zhu, 2011). Our results support these findings, showing an increase to C_3 photosynthetic efficiency and assimilation rate at CA conversion efficiencies (η_{CA}) above 10^3 (Figure 2). The gain reaches 10% at $\eta_{CA} = 10^6$ and begins to saturate at larger η_{CA}. Interestingly, the effect is essentially independent of the envelope permeability value, as long as we are not close to the compensation

5

point (Supplementary Figure 1). The results are similar when CA is expressed both in the chloroplast stroma and in the cytoplasm, but with a somewhat larger increase in C_3 efficiency and assimilation ($\sim 14\%$ at $\eta_{CA} = 10^6$, Figure 2).

With a C_4 cycle expressed, changing the efficacy of the cytoplasmic CA[3] can greatly affect photosynthesis (Supplementary Figure 2). Cytoplasmic CA activity acts as one of the bottlenecks to the pump throughput; for $\eta_{CA} < 10^4$ the pump is effectively non-operational and varying the PEPC level produces no noticeable change in the photon cost or the assimilation rate. For η_{CA} beyond 10^6, CA ceases to be a limiting factor at PEPC concentrations below 1 mM. Hence, we select $\eta_{CA} = 10^6$ as a default value both for cytoplasm and stroma. Depending on how effective the CA strain is, an η_{CA} of 10^6 would correspond to a CA active site concentration of 0.2 mM (spinach CA; Pocker and Ng (1973)) or ~ 1 mM (pea; Johansson and Forsman (1994)).

The impact of the gas permeability of the plastid envelope

We next investigate how the photon cost and assimilation rate depend on the envelope permeability and the PEPC concentration (i.e. the pump activity), Figure 3. Both photon cost and assimilation rate begin to change notably when PEPC concentration reaches $10^{-2} - 10^{-1}$ mM. By 1 mM, the efficacy measures saturate, as the pump reaches full activity. Taking into account the volume of the plastid and the surrounding cytoplasm, the PEPC concentration range of $10^{-2} - 10^{-1}$ mM corresponds to a PEPC-to-RubisCO carboxylation capacity ratio between 0.1 and 1, while saturation occurs at ratios close to 10. By comparison, the PEPC/RubisCO activity ratio in C_4 plants is between 2 and 6.5 (von Caemmerer et al., 2014). The reason behind the saturation in the photosynthetic activity at high PEPC concentrations is a limitation in the carbon supply - either the CA-assisted $CO_2 \leftrightarrow HCO_3^-$ conversion rate becomes insufficient or the diffusion of CO_2 from IAS through the cell wall reaches its limit.[4] Realistically however, we can expect that energy expenditure will limit photosynthesis before that, as we demonstrate later.

Of particular interest is how the photon cost changes with the pump activity level at different permeability values. At envelope permeabilities (σ_P) below a threshold value of $\sim 300\,\mu$m/s, the photon cost decreases when the pump is operational. Above the threshold permeability the opposite happens. At low envelope permeabilities the C_4 pathway would therefore be cost-efficient compared to C_3 photosynthesis. However, this regime is unlikely to occur in reality. To confirm this we can look at the photon cost at negligible PEPC concentration (that is, during C_3 photosynthesis). With the cell boundary permeability fixed at $200\,\mu$m/s, the photon cost of C_3 photosynthesis reaches 20/C for envelope permeability $\sigma_P \approx 600\,\mu$m/s (Figure 3), i.e. the actual permeability of the chloroplast envelope is higher than the $300\,\mu$m/s threshold and the photon cost of C_4 photosynthesis is higher than of C_3 photosynthesis. We note however that the threshold permeability value, where the C_4 pathway breaks-even, changes with CO_2 pressure in the internal airspaces, moving to higher values as the pressure decreases (see Supplementary Figure 3). Consequently, even for

---

[3] Here we only vary the efficacy of cytoplasmic CA, while keeping the efficacy of stromal CA fixed at 10^6.

[4] Depending on the particular values of η_{CA} and the permeability of the cellular boundary (σ_C), one or the other will form a bottleneck first. The relevant rates are the $CO_2 \rightarrow HCO_3^-$ conversion rate and the volume-adjusted rate of CO_2 diffusion from IAS ($\frac{A_C}{V_C}\sigma_C$, where A_C is the cell surface area and V_C is the volume of the peripheral cytoplasm). For default choice of parameter values (including $\eta_{CA} = 10^6$), these are roughly $4 \cdot 10^4\,\text{s}^{-1}$ and $500\,\text{s}^{-1}$, so the diffusion of CO_2 from the internal airspaces is limiting. At $\eta_{CA} = 10^4$ the conversion rate is only $400\,\text{s}^{-1}$ so it becomes limiting instead.

realistic envelope permeability values (i.e. several hundred μm/s) the proposed pathway *can* become a cost-efficient strategy under conditions of CO_2 deprivation (IAS CO_2 pressure $p_{CO_2} < 150\,\mu$bar, such as may occur during prolonged stomata closure).

Although the C_4 cycle may not be cost-effective in terms of quantum efficiency, it always increases the assimilation rate at sufficiently high PEPC activities. The gain can be substantial - up to several-fold at high PEPC concentrations - assuming photosynthesis is not limited by light (Figure 3(b)). The light-harvesting capacity of a plastid can be established by looking at the energy consumption of C_3 photosynthesis when the photon cost is not larger than 20/C ($\sigma_P \gtrsim 600\,\mu$m/s). We can see from Figure 3(b) that the light-harvesting capacity should be larger than 30 mM/s of photosynthetically active photons per stromal volume. We take 40 mM/s as a rough estimate of the actual, or at least easily achievable light-harvesting capacity of an average plastid. As we demonstrate later, significant assimilation gains are feasible even at this limited capacity.

The impact of other variables

The impact of the vacuole membrane permeability on the C_4 cycle efficiency is minimal (Supplementary Figure 4), although changing the thickness of the peripheral cytoplasmic layer does change the cytoplasmic PEPC concentration at which a particular efficiency or gain level is achieved (Supplementary Figure 4(c)). It appears that what really matters is the total amount of PEPC in the cytoplasm compared with RubisCO in the plastids (Supplementary Figure 4(d)).

Changing the permeability of the cell wall and plasmalemma (σ_C) results in significant changes to the photon cost and the assimilation rate, as one could expect (Supplementary Figure 5). The efficacy of the C_4 cycle (that is, its advantage or disadvantage over C_3 photosynthesis) is only slightly affected, however. At very high σ_C, the C_4 cycle allows for a several-fold higher assimilation rate, as the bottleneck due to diffusion of CO_2 through the cell wall is removed, but a concurrent increase in the photon cost means the plastid light-harvesting capacity would be limiting. This can be noted in the capacity thresholds which follow the assimilation rate isolines at high σ_C in Supplementary Figure 5(b).

Changing the chloroplast surface coverage (Figure 4) leads to an interesting result: while the activation of the C_4 pump (when the envelope permeability is above the break-even threshold) will always cause the photon cost to rise, for lower surface coverages ($30\% - 50\%$) this rise is less steep. A remarkable and non-intuitive consequence is that higher assimilation rate *per cell surface area* (and hence *per leaf-surface area*, assuming a fixed mesophyll-to-leaf surface ratio) can be achieved at lower chloroplast surface coverage, i.e. at a lower investment in plastids (Figure 4(b)).

Increasing the plastid size while keeping the cell surface coverage constant (Figure 5) means more RubisCO per cell surface area and hence a higher assimilation rate, but also a higher photon cost due to the increased RuBP oxygenation in the case of C_3 photosynthesis. The C_4 cycle, at high enough PEPC concentrations, can reverse this negative trend. At PEPC-to-RubisCO capacity ratios above 3, C_4 efficiency increases with plastid size, although C_4 photosynthesis still remains less efficient than C_3 photosynthesis, except for unrealistically large plastids. This results

7

in a higher assimilation rate per cell-surface area combined with lower demands on the light-harvesting capacity (Figure 5(b)).

The gain under realistic light utilisation limits

We now examine what gains are achievable when the energy input is a constraining factor. This could be either due to limited light availability or limited light-harvesting capacity. We expect that at energy inputs below the level needed to operate C_3 photosynthesis, activating the C_4 pump would negatively affect the assimilation rate. Therefore we consider only situations where the energy constraints do not inhibit C_3 photosynthesis. This will be the case at light-utilisation caps of 40 mM/s or more. If the thylakoid surface area is not the constraining factor in C_3 photosynthesis, it should be possible to boost the plastid light-harvesting capacity well beyond 40 mM/s by overexpressing the photosystem complexes and associated proteins on the thylakoid. We examine photosynthesis under a realistic light-utilisation cap of $\sim$ 40 mM/s, and under a *reasonably* optimistic one of 80 mM/s. These correspond to a utilisation of 2% and 4% of the maximal incident solar flux on the plastid.[5]

Figure 6(a) shows how assimilation changes with the PEPC concentration at different envelope permeabilities, when the 40 mM/s cap is imposed. The steady-state operation is not affected as long as energy use remains below the cap. When energy availability becomes limiting there is a reduction in the concentrations of available RuBP-primed RubisCO and PEP-primed PEPC. As their carboxylation capacity ratio remains constant (by assumption), the operation under an energy constraint will be the same as unconstrained operation at a reduced, effective RubisCO concentration, with the same PEPC-to-RubisCO ratio. High PEPC concentration will then result in reduced assimilation, as the C_4 cycle and Calvin-Benson cycle enzymes compete for energy resources. We might then expect that the optimal assimilation under an energy constraint is achieved exactly at the threshold where the energy usage reaches the cap. This is essentially the case for the 80 mM/s cap, but is not generally true. As the C_4 cycle changes the operating conditions in the stroma (i.e. CO_2 levels) this can result in a situation where a lower effective RubisCO concentration results in a higher net assimilation. The comparison of the assimilation gains (with respect to C_3 photosynthesis) at the threshold PEPC concentration where the energy consumption reaches the cap, and at the concentration where the optimal assimilation is accomplished is shown in Figure 6(b). The respective PEPC concentrations are shown in Figure 6(c). It is evident that the C_4 cycle activity has to be tuned to obtain the maximal benefit. Given that light supply fluctuates continually, dynamic control of the C_4 cycle activity would have to be implemented. Alternatively, under-operating the cycle (i.e. having its activity level below the speculated optimum) may be a beneficial strategy.

Even without a fine-tuned C_4 cycle a sizeable gain in the assimilation rate can be expected as long as envelope permeability is not too large. Looking at the photosynthetic performance at the threshold where the energy consumption reaches the 40 mM/s cap, we predict that up to 20% gain in carbon assimilation at the permeability of 600 μm/s may be achieved, with the photon cost rising by less than 10%. With the higher LHC of 80 mM/s (and sufficient sunlight) large gains are possible over the entire range of the envelope permeability values. Assimilation may even be doubled.

---

[5]Or 1% and 2% of solar flux incident on cell surface (at 50% chloroplast surface coverage).

Stomatal conductance is continually tuned to the environment and when conductances are low photosynthesis is frequently CO_2 deprived. Assimilation gains from using the C_4 pump are much more prominent at low CO_2 pressures in the internal airspaces, Figure 7(a). At $120\,\mu$bar CO_2 the assimilation could be doubled, while still not exceeding the $40\,$mM/s light-utilisation cap (Figure 7(b)). In contrast, at $400\,\mu$bar no gain is possible with that energy cap (Figure 7(b)).

Discussion

We modelled a hypothetical cytoplasm-to-stroma C_4 cycle in a C_3 mesophyll cell geometry, and quantified carbon assimilation and photosynthetic efficiency. The proposed C_4 pump would lead to an increase in assimilation rate whenever there is sufficient light-harvesting capacity *and* excess light is available. The magnitude of this gain is highly dependent on CO_2 permeability of the chloroplast envelope and on operating conditions, such as the internal airspace CO_2 pressure and light availability. At medium envelope permeability ($600\,\mu$m/s), CO_2 pressure ($250\,\mu$bar), and light-harvesting capacity ($40\,$mM/s), the gain is moderate (20%). At low CO_2 pressure ($125\,\mu$bar), or at high light availability and harvesting capacity ($80\,$mM/s), the gain becomes significant (85%), Figure 7(b). Due to the design of the model, which assumes optimal functioning of the C_3/C_4 enzymatic pathways, these predictions always represent the best case scenario. Even so, the massive predicted assimilation advantage under conditions of CO_2 deprivation is unlikely to be spurious. As CO_2 deprivation is a common hazard facing plants in dry and warm climates - which are typically well-lit - the development of the proposed C_4 pathways could be *very* beneficial for creating drought-resistant high-yield crop strains. Regarding this it is interesting to note that terrestrial species that *have* evolved single-celled C_4 photosynthesis grow in salty depressions in semi-arid regions - the conditions that would likely lead to low CO_2 within the leaf (Voznesenskaya et al., 2001, 2002).

Ideally a regulation mechanism should be incorporated to moderate the activity of the C_4 pump based on the energy availability, so as to prevent it from competing adversely with the Calvin-Benson cycle. Regulation of the C_4 cycle based on the ambient light levels and CO_2 availability is already present in Kranz-type C_4 plants (Furbank and Taylor, 1995), so simply implementing existing C_4 regulatory mechanisms may allow this.

Our conclusions are generally in qualitative agreement with von Caemmerer (2003), but our detailed examination of parameter space produces more positive results, inspiring greater optimism. As Figure 6(b) shows, predicted gains from the C_4 cycle are much higher at lower envelope permeabilities. Likewise, although we agree with von Caemmerer (2003) that the C_4 cycle will be cost-inefficient, the difference between carbon assimilation costs in C_3 and C_4 photosynthesis is smaller at lower envelope permeability, and, as we demonstrate by evaluating the expected assimilation at limited light-harvesting ability, the operation of a C_4 cycle need not be prohibitively expensive.

To elucidate the differences in our conclusions, we attempt a more direct comparison with the results of von Caemmerer and Furbank (2003). At $200\,$ppm CO_2 in the IAS, they predict that operating the C_4 pump at 1:1 PEPC-to-RubisCO carboxylation capacity ratio would result in a 40% increase in the assimilation rate and a 70% increase in energy cost per assimilated carbon (Figure 5 in von Caemmerer and Furbank (2003)). Their model expresses gas

conductances and enzyme catalytic capacities per leaf-surface area, so a comparison requires an assumption of the mesophyll-to-leaf surface area ratio. Using a ratio of 13.5 (the value is similar to the ratios found for A. thaliana (8-10) by Tholen et al. (2008)), the RubisCO catalytic capacities in the two models match,[6] so we use this value for the comparison. Their conductances then correspond to permeabilities of the envelope, and of the cell wall and plasmalemma, of approximately $10^3 \, \mu$m/s each. With the same parameters we get a 50% increase in the assimilation rate with a 30% increase in the photon cost (from 17/C to 22/C). There is a significant difference in the predictions of the energy cost of C_4 photosynthesis. The difference likely stems from different accounting methods - von Caemmerer and Furbank (2003) consider ATP consumption whereas our quantification in terms of light-use factors in the fact that the C_4 cycle does not need a reductive agent so its ATP requirements can be met by the cyclic electron transfer chain, which is more efficient at creating a proton gradient across thylakoid membrane, and thus ATP production per photon is higher.

Another promising result is that the pathway's beneficial effects can be increased further by reducing the chloroplast surface coverage, bringing it into the region in Figure 4(a) where the rise in the photon cost when the C_4 pump is active is less pronounced. This minor change to the cell anatomy would allow for the same assimilation rate to be achieved with a reduced plastid investment, translating into an even higher plant growth rate. One way this could be accomplished might be to arrest or slow down the chloroplast division cycle. A possible side-effect would be an increase in the average plastid size, which would further benefit C_4 photosynthesis (Figure 5). An illustration of possible benefits from a design strategy that combines the implementation of a C_4 cycle with alterations in the chloroplast surface coverage is presented in Figure 8. The design steps are broadly outlined in Figure 8(b). Figure 8(a) shows how the assimilation rate varies with the surface coverage (assuming no changes in the plastid size) for C_3 photosynthesis, and C_4 photosynthesis at 40 mM/s and 80 mM/s light utilisation thresholds (compare with Figure 4(b)). Starting with C_3 photosynthesising plastids at 50% cell surface coverage (a_0), implementing the C_4 pump and boosting the light-harvesting capacity to 40 mM/s (a_1) or 80 mM/s (a_2) would result in a 15% or an 85% increase in the assimilation rate respectively. Alternatively, at 40 mM/s light-harvesting capacity, the number of plastids could be reduced by 20% (b_1) without any loss in assimilation compared to C_3 photosynthesis. Boosting the light-harvesting capacity to 80 mM/s would allow for a 65% increase in the assimilation rate with 20% fewer plastids (b_2), or alternatively, for a 60% reduction in the number of plastids without a decrease in assimilation (c_2). If the plastids are also enlarged in the process, even larger gains may be possible. The level of required C_4 cycle expression, quantified by the PEPC/RubisCO carboxylation capacity ratio, would not need the exceed the observed level of C_4 cycle activity in C_4 plants (2-7; von Caemmerer et al. (2014)), even at 80 mM/s light-harvesting capacity (Figure 8(a)). The relative expression of the two photosystems may need to be rebalanced however, to allow for a larger cyclic electron current through PS-I (Figure 8(a)). The optimal modification strategy would be the one that maximises the return on resource investment. To calculate this however, the maintenance costs also need to be established. Quantifying the return-on-investment

---

[6]The RubisCO activity in von Caemmerer and Furbank (2003) is $100 \, \mu$mol/m^{2}s, and the gas conductances of the envelope and the cell wall are 0.8 mol/bar m^{2}s each.

and deciding the optimal strategy will require additional research.

Acknowledgements

References

Badger, M., Aug. 2003. The roles of carbonic anhydrases in photosynthetic CO2 concentrating mechanisms. Photosynthesis Research 77 (2-3), 83.

Björkman, O., Demmig-Adams, B., 1995. Regulation of Photosynthetic Light Energy Capture, Conversion, and Dissipation in Leaves of Higher Plants. In: Schulze, P. D. E.-D., Caldwell, P. D. M. M. (Eds.), Ecophysiology of Photosynthesis. No. 100 in Springer Study Edition. Springer Berlin Heidelberg, pp. 17–47, dOI: 10.1007/978-3-642-79354-7_2.

Carroll, J. J., Slupsky, J. D., Mather, A. E., 1991. The Solubility of Carbon Dioxide in Water at Low Pressure. Journal of Physical and Chemical Reference Data 20 (6), 1201.

Cousins, A. B., Ghannoum, O., von Caemmerer, S., Badger, M. R., Mar. 2010. Simultaneous determination of Rubisco carboxylase and oxygenase kinetic parameters in *Triticum aestivum* and *Zea mays* using membrane inlet mass spectrometry. Plant, Cell & Environment 33 (3), 444–452.

Ehleringer, J., Pearcy, R. W., Nov. 1983. Variation in Quantum Yield for CO2 Uptake among C3 and C4 Plants. Plant Physiol. 73 (3), 555–559.

Ellis, J. R., Leech, R. M., Jul. 1985. Cell size and chloroplast size in relation to chloroplast replication in light-grown wheat leaves. Planta 165 (1), 120–125.

Evans, J. R., Kaldenhoff, R., Genty, B., Terashima, I., May 2009. Resistances along the CO2 diffusion pathway inside leaves. Journal of Experimental Botany 60 (8), 2235–2248.

Fabre, N., Reiter, I. M., Becuwe-Linka, N., Genty, B., Rumeau, D., May 2007. Characterization and expression analysis of genes encoding α and β carbonic anhydrases in Arabidopsis. Plant, Cell & Environment 30 (5), 617–629.

Falkowski, P. G., Raven, J. A., Oct. 2013. Aquatic Photosynthesis: Second Edition. Princeton University Press, google-Books-ID: kU-CrAQAAQBAJ.

Furbank, R., Taylor, W., Jul. 1995. Regulation of Photosynthesis in C3 and C4 Plants: A Molecular Approach. Plant Cell 7 (7), 797–807.

Furbank, R. T., von Caemmerer, S., Price, G. D., Dec. 2013. CO2-concentrating mechanisms in crop plants to increase yield. In: Gready, J. E., Dwyer, S. A., Evans, J. R. (Eds.), Applying photosynthesis research to improvement of food crops. Australian Centre for International Agricultural Research (ACIAR), pp. 130–137.

Johansson, I.-M., Forsman, C., Sep. 1994. Solvent Hydrogen Isotope Effects and Anion Inhibition of CO2 Hydration Catalysed by Carbonic Anhydrase from Pisum sativum. European Journal of Biochemistry 224 (3), 901–907.

Jurić, I., González-Pérez, V., Hibberd, J. M., Edwards, G., Burroughs, N. J., Jan. 2017. Size matters for single-cell C4 photosynthesis in Bienertia. J Exp Bot 68 (2), 255–267.

Kai, Y., Matsumura, H., Inoue, T., Terada, K., Nagara, Y., Yoshinaga, T., Kihara, A., Tsumura, K., Izui, K., Feb. 1999. Three-dimensional structure of phosphoenolpyruvate carboxylase: A proposed mechanism for allosteric inhibition. PNAS 96 (3), 823–828.

Kaldenhoff, R., Kai, L., Uehlein, N., May 2014. Aquaporins and membrane diffusion of CO2 in living organisms. Biochimica et Biophysica Acta (BBA) - General Subjects 1840 (5), 1592–1595.

Mazarei, A. F., Sandall, O. C., Jan. 1980. Diffusion coefficients for helium, hydrogen, and carbon dioxide in water at 25C. AIChE J. 26 (1), 154–157.

Missner, A., Kügler, P., Saparov, S. M., Sommer, K., Mathai, J. C., Zeidel, M. L., Pohl, P., Sep. 2008. Carbon Dioxide Transport through Membranes. J. Biol. Chem. 283 (37), 25340–25347.

Murray, C. N., Riley, J. P., Jun. 1969. The solubility of gases in distilled water and sea water—II. Oxygen. Deep Sea Research and Oceanographic Abstracts 16 (3), 311–320.

Pocker, Y., Ng, J. S. Y., Dec. 1973. Plant carbonic anhydrase. Properties and carbon dioxide hydration kinetics. Biochemistry 12 (25), 5127–5134.

Sage, R. F., Feb. 2004. The evolution of C4 photosynthesis. New Phytologist 161 (2), 341–370.

Terashima, I., Hanba, Y. T., Tazoe, Y., Vyas, P., Yano, S., Jan. 2006. Irradiance and phenotype: comparative eco-development of sun and shade leaves in relation to photosynthetic CO2 diffusion. J. Exp. Bot. 57 (2), 343–354.

Tholen, D., Boom, C., Noguchi, K., Ueda, S., Katase, T., Terashima, I., Nov. 2008. The chloroplast avoidance response decreases internal conductance to CO2 diffusion in Arabidopsis thaliana leaves. Plant, Cell & Environment 31 (11), 1688–1700.

Tholen, D., Zhu, X.-G., May 2011. The Mechanistic Basis of Internal Conductance: A Theoretical Analysis of Mesophyll Cell Photosynthesis and CO2 Diffusion. Plant Physiol. 156 (1), 90–105.

Tiwari, A., Kumar, P., Singh, S., Ansari, S. A., Mar. 2005. Carbonic anhydrase in relation to higher plants. Photosynthetica 43 (1), 1–11.

Tsuzuki, M., Miyachi, S., Edwards, G. E., Jul. 1985. Localization of Carbonic Anhydrase in Mesophyll Cells of Terrestrial C3 Plants in Relation to CO2 Assimilation. Plant Cell Physiol 26 (5), 881–891.

Uehlein, N., Otto, B., Hanson, D. T., Fischer, M., McDowell, N., Kaldenhoff, R., Mar. 2008. Function of Nicotiana tabacum Aquaporins as Chloroplast Gas Pores Challenges the Concept of Membrane CO2 Permeability. Plant Cell 20 (3), 648–657.

von Caemmerer, S., 2000. Biochemical models of leaf photosynthesis. No. 2 in Techniques in plant science. CSIRO, Collingwood.

von Caemmerer, S., Aug. 2003. C4 photosynthesis in a single C3 cell is theoretically inefficient but may ameliorate internal CO2 diffusion limitations of C3 leaves. Plant, Cell and Environment 26 (8), 1191–1197.

von Caemmerer, S., Edwards, G. E., Koteyeva, N., Cousins, A. B., Aug. 2014. Single cell C4 photosynthesis in aquatic and terrestrial plants: A gas exchange perspective. Aquatic Botany 118, 71–80.

von Caemmerer, S., Furbank, R. T., 2003. The C4 pathway: an efficient CO2 pump. Photosynthesis Research 77 (2-3), 191–207.

Voznesenskaya, E. V., Franceschi, V. R., Kiirats, O., Artyusheva, E. G., Freitag, H., Edwards, G. E., Sep. 2002. Proof of C4 photosynthesis without Kranz anatomy in Bienertia cycloptera (Chenopodiaceae). The Plant Journal 31 (5), 649–662.

Voznesenskaya, E. V., Franceschi, V. R., Kiirats, O., Freitag, H., Edwards, G. E., Nov. 2001. Kranz anatomy is not essential for terrestrial C4 plant photosynthesis. Nature 414 (6863), 543–546.

Xiao, Y., Tholen, D., Zhu, X.-G., Nov. 2016. The influence of leaf anatomy on the internal light environment and photosynthetic electron transport rate: exploration with a new leaf ray tracing model. J Exp Bot 67 (21), 6021–6035.

Zhu, X.-G., Long, S. P., Ort, D. R., Apr. 2008. What is the maximum efficiency with which photosynthesis can convert solar energy into biomass? Current Opinion in Biotechnology 19 (2), 153–159.

Zhu, X.-G., Long, S. P., Ort, D. R., Jun. 2010. Improving Photosynthetic Efficiency for Greater Yield. Annual Review of Plant Biology 61 (1), 235–261.
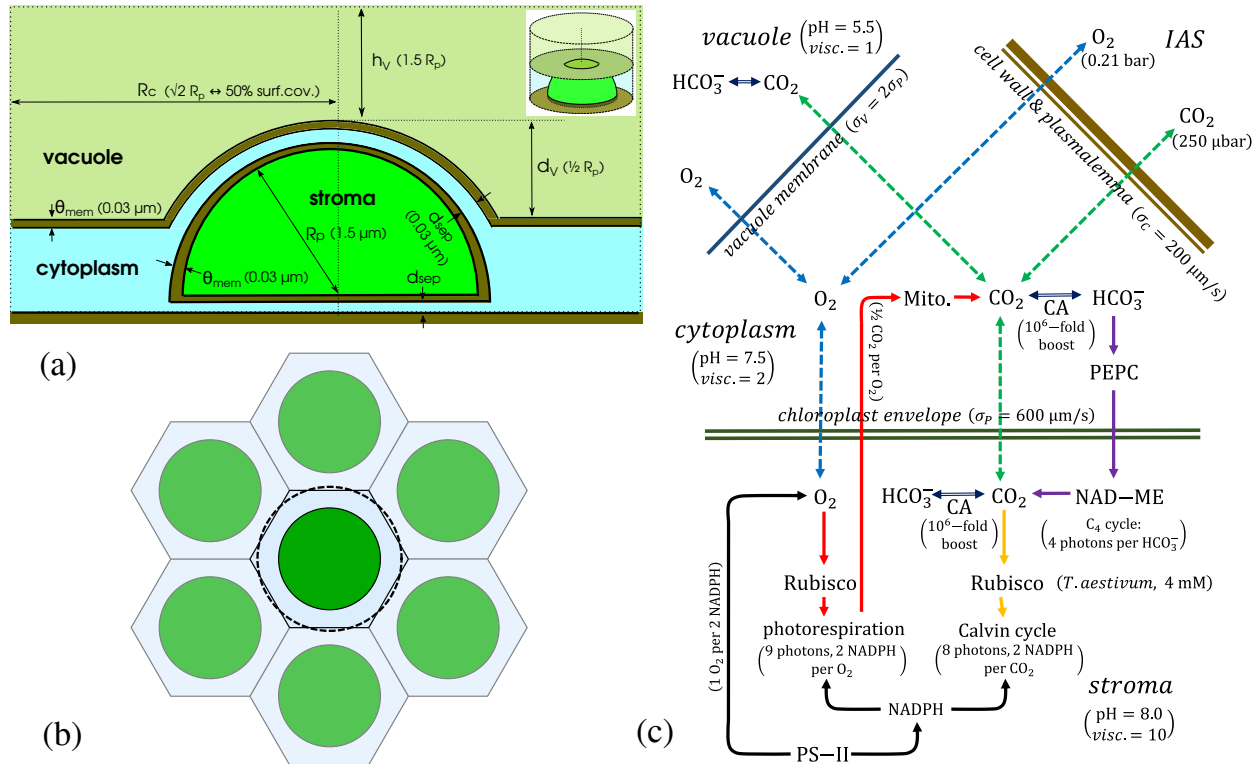
12

Figure 1: The spatial single-cell C_4 photosynthesis model. (a): the cross-section of the simulated cylindrical volume (insert) containing a semi-spherically shaped plastid, the peripheral cytoplasm, and a part of the vacuole interior (not to scale). The cylinder radius is determined by the plastid surface coverage. (b): The cylindrical symmetry approximates the 'personal' space of an individual plastid in a roughly hexagonal close-packed arrangement of plastids in the areas of mesophyll surface adjacent to IAS. The panel shows such an arrangement at 50% surface coverage ratio. The simulated cylinder is represented by the dashed circle. (c): A schematic representation of the physical processes and chemical pathways modelled. O_2, CO_2, and HCO_3^- can freely diffuse within individual regions, but O_2 and CO_2 can also diffuse through interregional boundaries (dashed green and blue arrows). Depending on the region, the interconversion of CO_2 and HCO_3^- (dark blue arrows) proceeds with or without CA assistance. CO_2 reacting with RuBP-primed RubisCO drives the Calvin cycle (orange arrows). O_2 reacting with RuBP-primed RubisCO activates the photorespiratory pathway (red arrows). HCO_3^- reacting with PEP-primed PEPC is the starting point for the carbon transport through the C_4 pathway (purple arrows). Oxygen production at PS-II is coupled to the NADPH consumption in the Calvin and photorespiratory cycles (black arrows). Parentheses in (a) and (c) show the default parameter values.

13

Table 1: The list of parameters used in the model and in calculation of derived measures. Where not explicitly varied, the parameters are fixed at their default values.

| Parameter	Symbol	Default value	Note
Plastid radius	r_P	$1.5\,\mu m$	From Ellis and Leech (1985)
Chloroplast surface coverage	$\phi_{P/C}$	50%	From Ellis and Leech (1985)
Envelope-plasmalemma / envelope-tonoplast membrane separation	d_{sep}	$0.03\,\mu m$	
Envelope and tonoplast membrane thickness	θ_{mem}	$0.03\,\mu m$	The membrane thickness is exaggerated to improve numeric convergence. It does not affect the results except through excluded volume.
Vacuole drop	d_V	$\frac{1}{2}r_P$	The depth by which the plastid 'projects' into the vacuole space (see Fig. 1(a)).
Vacuole height	h_V	$1.5 \times r_P$	The height (along the central axis) of the simulated part of the vacuole space.
RubisCO active site concentration	c_R	4 mM	Known range is $2\,\text{mM}$-$5\,\text{mM}$ (von Caemmerer, 2000)
PEPC active site concentration	c_P	variable	
RubisCO carboxylation catalysis rate	k_{catRC}	$3.8\,\text{s}^{-1}$	
RubisCO oxygenation catalysis rate	k_{catRO}	$0.83\,\text{s}^{-1}$	For *T. aestivum* from Cousins et al. (2010)
RubisCO Michaelis concentration for CO_2	K_{RC}	$9.7\,\mu M$	
RubisCO Michaelis concentration for O_2	K_{RO}	$244\,\mu M$	
PEPC carboxylation catalysis rate	$k_{catPbiC}$	$150\,\text{s}^{-1}$	For *Z. mays* from Kai et al. (1999)
PEPC Michaelis concentration for HCO_3^-	K_{PbiC}	$100\,\mu M$	
CO_2 pressure in the IAS	p_{CO_2}	$250\,\mu bar$	
O_2 pressure in the IAS	p_{O_2}	0.21 bar	
Henry constant for CO_2 at 20^oC	ν_C	38.5 mM/bar	From dissolved concentrations at $400\,\mu bar$ and
Henry constant for O_2 at 20^oC	ν_O	1.36 mM/bar	210 mbar taken from Carroll et al. (1991) and Murray and Riley (1969).
pH in chloroplast stroma		8.0	
pH in the cytoplasm		7.5	
pH within the vacuole		5.5	
$CO_2 \leftrightarrow HCO_3^-$ conversion rate boost due to CA	η_{CA}	10^6	Saturating, see text.
Combined permeability of the cell wall and plasmalemma to O_2 and CO_2	σ_C	$200\,\mu m/s$	Ranges in literature from 2 to $5 \cdot 10^3\,\mu m/s$ (Evans et al., 2009; Terashima et al., 2006).
Permeability od the chloroplast envelope to O_2 and CO_2	σ_P	$600\,\mu m/s$	Ranges in literature from $20\,\mu m/s$ (Uehlein et al., 2008) to $> 3.6\,cm/s$ (Missner et al., 2008).
Permeability od the tonoplast membrane to O_2 and CO_2	σ_V	$2\sigma_P$	Assumed to have similar properties to the membranes forming the envelope.
Permeability of the chloroplast envelope to HCO_3^-		1 nm/s	Essentially zero.
Permeability od the tonoplast membrane to HCO_3^-		2 nm/s	
Diffusion constant for CO_2 in water	$D_{C,aq}$	$1800\,\mu m^2/s$	From Mazarei and Sandall (1980)
Diffusion constant for O_2 in water	$D_{O,aq}$	$1800\,\mu m^2/s$	From Mazarei and Sandall (1980)
Diffusion constant for HCO_3^- in water	$D_{biC,aq}$	$1100\,\mu m^2/s$	Falkowski and Raven (2013)
Cytoplasm viscosity relative to water	η_C	2	
Stroma viscosity relative to water	η_P	10	As in Tholen and Zhu (2011).
Vacuole interior viscosity relative to water	η_V	1	
Plastid light-harvesting capacity	LHC	Varied	Either unlimited, $40\,mM/s$, or $80\,mM/s$.
Base photon cost of RuBP regeneration	φ_{Calvin}	8	
Base photorespiration photon cost	φ_{phresp}	9	From Zhu et al. (2010)
Base cost of pyruvate-to-PEP conversion	φ_{C4}	4	

14
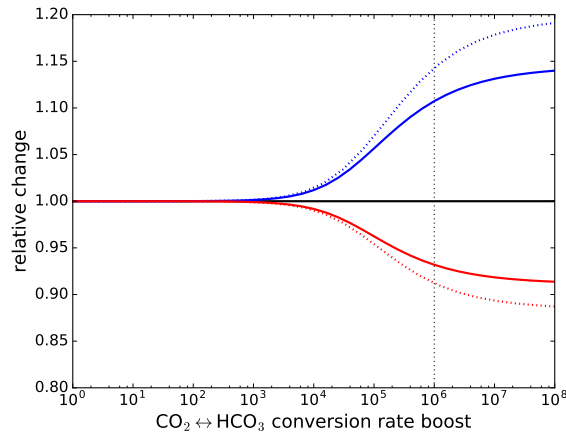
Figure 2: Cytoplasmic CA and C_3 photosynthesis. The assimilation rate gain (blue) and the photon cost reduction (red) as functions of CA effectiveness (η_{CA}) for $\sigma_P = 600\,\mu$m/s. Solid lines are for the case of CA present only in the plastid stroma; dashed lines are for the case of CA present both in the stroma and in the cytoplasm. The vertical dotted line marks the boost factor used as default in other figures.
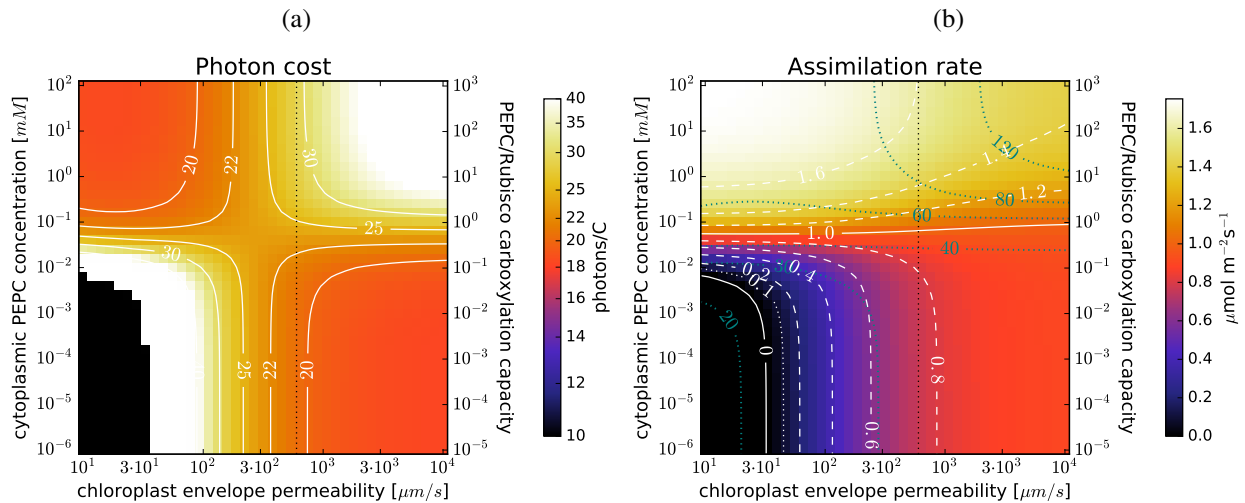

Figure 3: Envelope permeability and C_4 photosynthesis: The photon cost (a) and the net assimilation rate (b) as functions of the envelope permeability and PEPC concentration in the cytoplasm for the default parameter choice (Table 1). The purple lines in (b) mark the light-utilisation thresholds (in mM/s). In the black regions the photon cost and the assimilation rate are negative. The vertical dotted line marks the envelope permeability used as default in other figures.
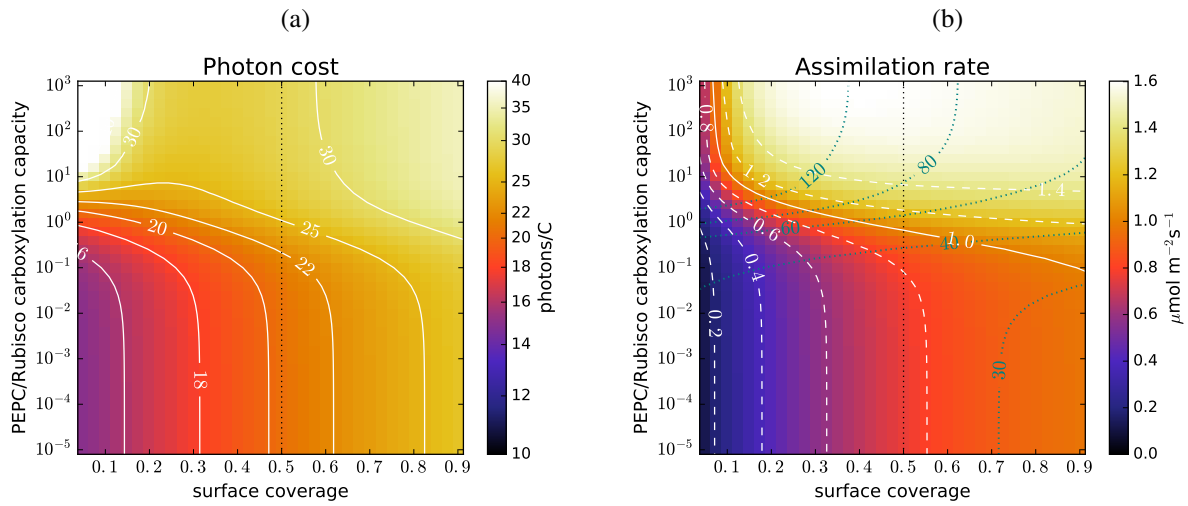
(a)

(b)

Figure 4: Plastid surface coverage and C_4 photosynthesis: The photon cost (a) and the net assimilation rate (b) as functions of the chloroplast surface coverage and PEPC-to-RubisCO carboxylation capacity ratio, for the default parameter choice (Table 1). The purple lines in (b) mark the light-utilisation thresholds (in mM/s). The carboxylation capacity ratio is used instead of the PEPC concentration to quantify the C_4 cycle activity because the cytoplasmic volume per plastid changes with the coverage. The vertical dotted line marks the surface coverage used as default in other figures.
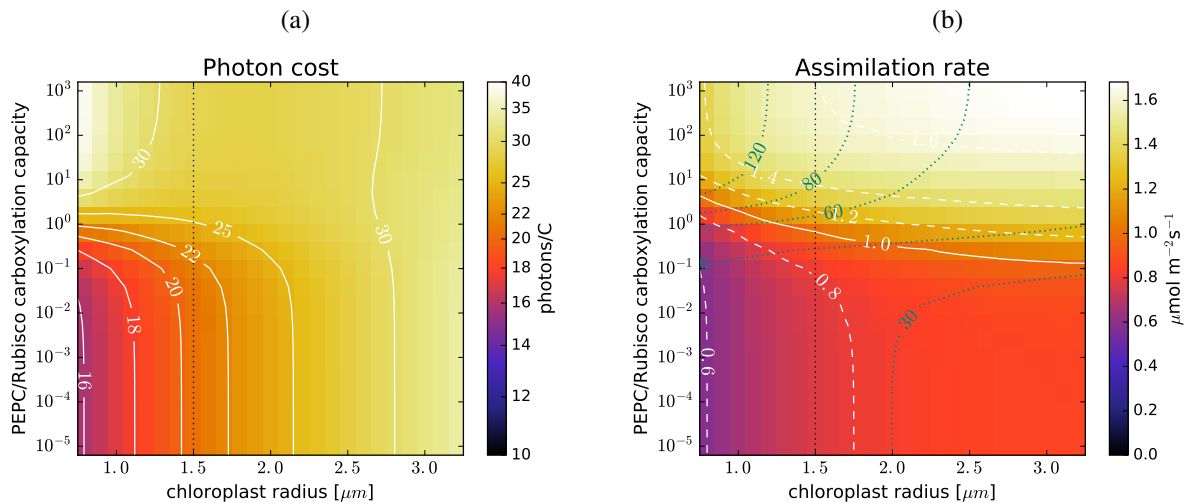
(a)

(b)

Figure 5: Plastid size and C_4 photosynthesis: The photon cost (a) and the net assimilation rate (b) as functions of the chloroplast radius and PEPC-to-RubisCO carboxylation capacity ratio, for the default parameter choice (Table 1). The purple lines in (b) mark the light-utilisation thresholds (in mM/s). The carboxylation capacity ratio is used instead of the PEPC concentration to quantify the C_4 cycle activity because the stromal volume per cell-surface area changes with plastid radius. The vertical dotted line marks the plastid size used as default in other figures.
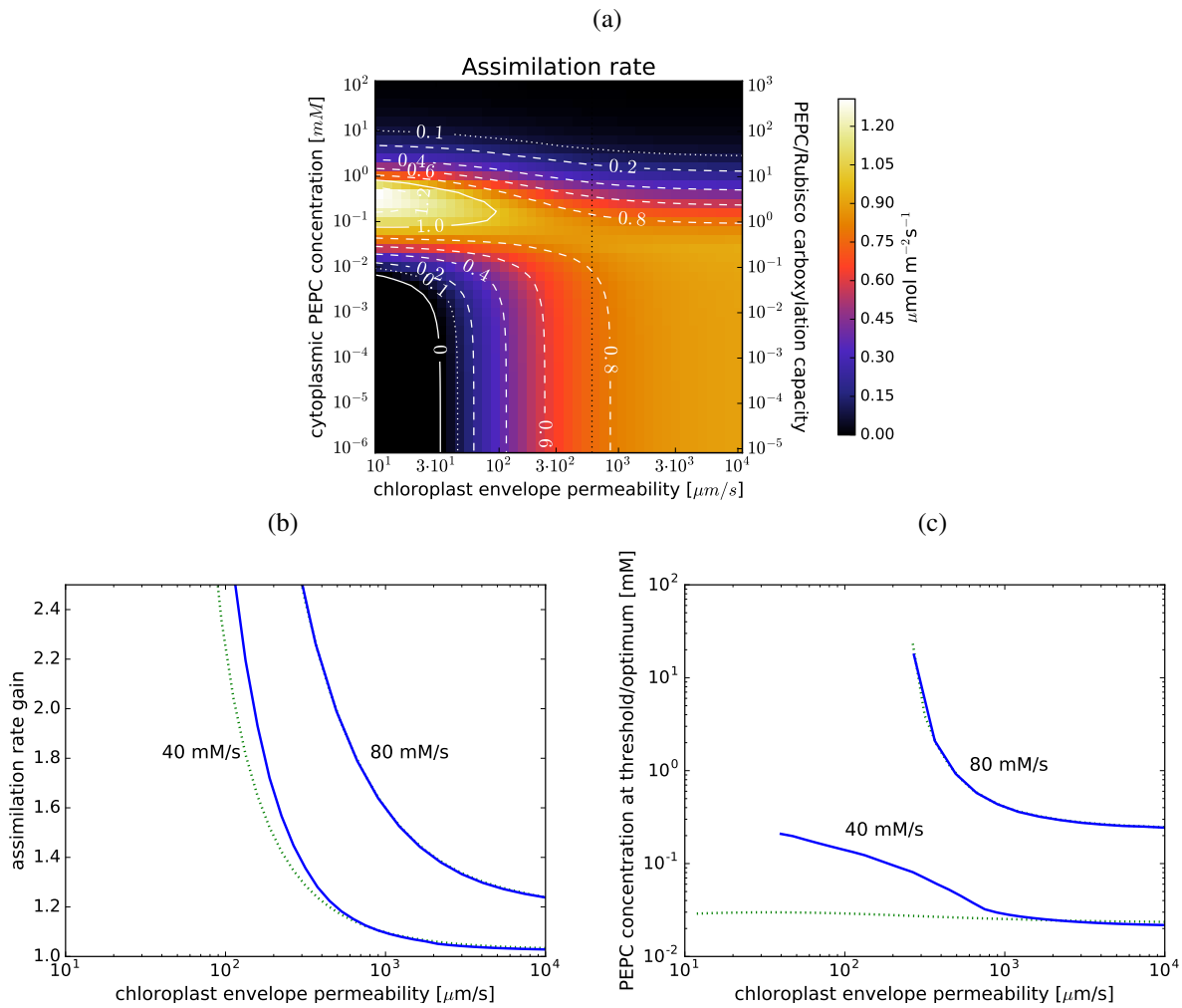
16

(a)

(b)   (c)

Figure 6: C$_4$ photosynthesis at limited light-harvesting capacity. (a): The net assimilation rate as a function of the envelope permeability and PEPC concentration in the cytoplasm when the light input is capped at 40 mM/s. Parameters as in Fig. 3. The vertical dotted line marks the permeability used as default in other figures. (b): The relative gain in the assimilation rate at the PEPC activity levels where the light usage reaches 40 mM/s and 80 mM/s (dotted green lines, corresponding to the purple lines in Fig. 3(b)) and the maximal assimilation gains when the caps are imposed (blue lines). (c): the respective PEPC concentrations at which the optimal gains are achieved.
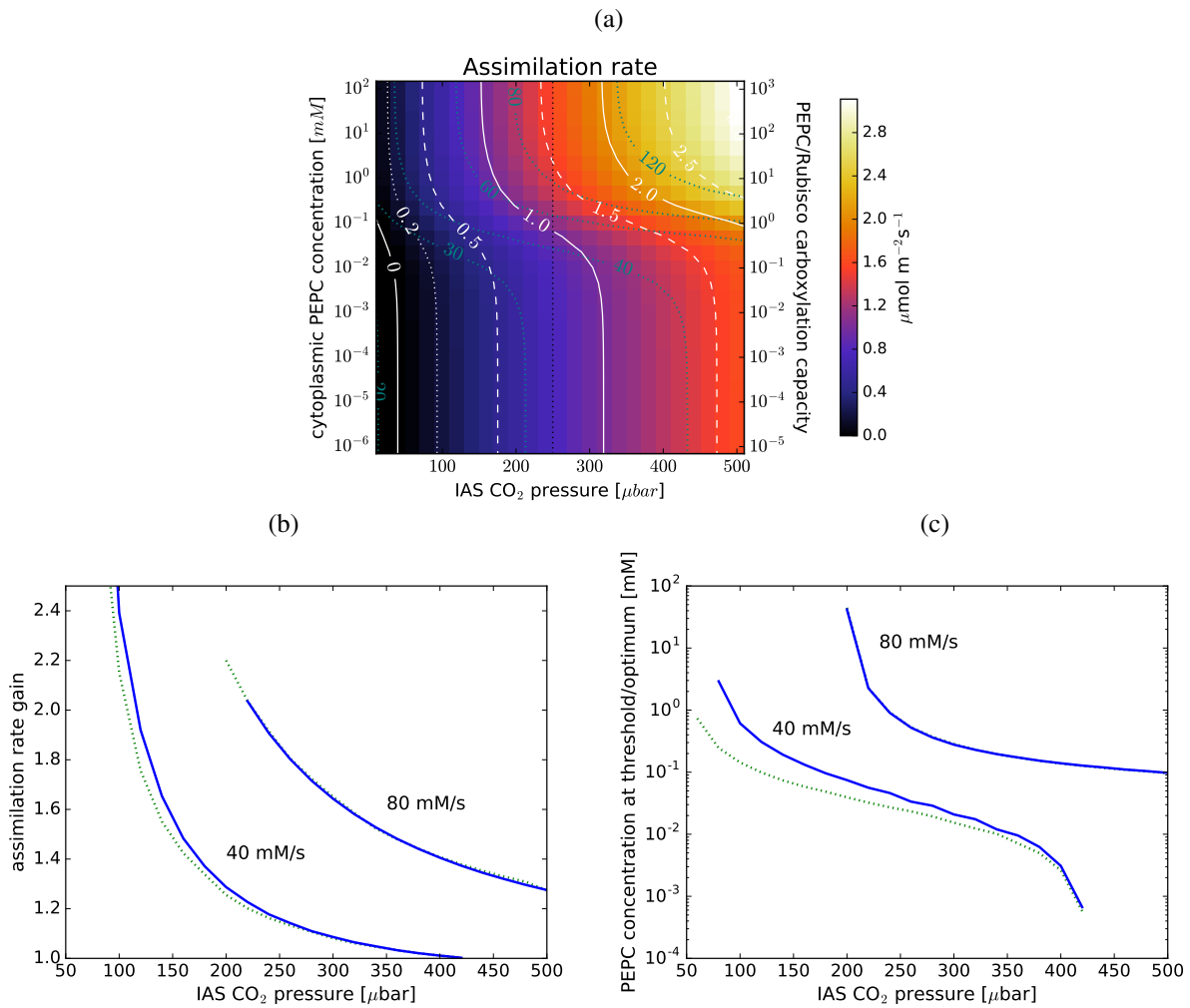
17

Figure 7: C_4 photosynthesis at limited CO_2 in the IAS. (a): The net assimilation rate as a function of the IAS CO_2 pressure and PEPC concentration in the cytoplasm, for the default parameter choice (Table 1). No light utilisation cap is imposed, but the utilisation thresholds are marked in purple. The vertical dotted line marks the CO_2 pressure used as default in other figures. (b): The relative gain in the assimilation rate at the PEPC activity levels where the light usage reaches 40 mM/s and 80 mM/s (dotted green lines) and the maximal assimilation gains when the caps are imposed (blue lines). (c): the respective PEPC concentrations at which the optimal gains are achieved.

18

(a)   (b)
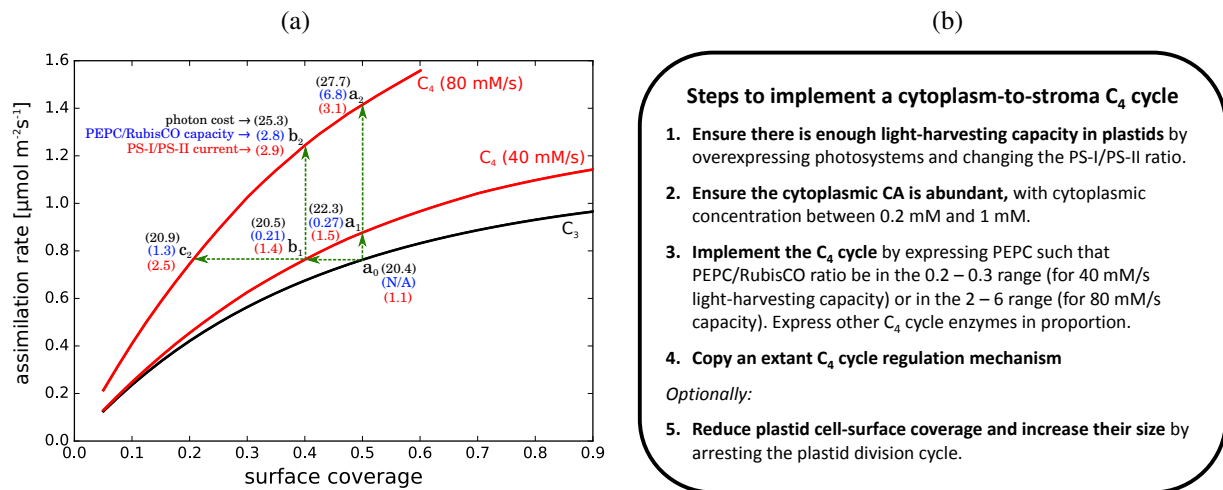

Figure 8: Altering plastid surface coverage and light harvesting capacity: (a) The assimilation rate per cell surface area as a function of chloroplast surface coverage in the case of C_3 photosynthesis (black line) and C_4 photosynthesis at the C_4 cycle activity levels where light-use reaches 40 mM/s and 80 mM/s thresholds (red lines). The numbers in parentheses show the respective photon costs (black), PEPC-vs-RubisCO carboxylation capacity ratios (blue), and ratios of electron current through PS-I and PS-II (red). Green arrows illustrate organism modification strategies discussed in the main text. Parameters as in Fig. 4. (b) An outline of a recipe for making a functional C_4 photosynthesising prototype.

19

Supplementary Information

Mathematical outline of the model

To find the gas currents under steady-state photosynthesis we need to solve the system of stationary diffusion-reaction equations for position-dependent concentrations of oxygen, carbon-dioxide, and bicarbonate - n_O, n_C, and n_{biC} - satisfying appropriate boundary constraints and flux-balance conditions. The equations are of the form

$$D_i \nabla^2 n_i - r_i(\boldsymbol{n}) + s_i = 0 \tag{1}$$

where the index i stand for C, O, and biC respectively. D_i is the compartment-dependent diffusion coefficient. r_i and s_i are the reaction and source terms. Both will depend on the location (the compartments, i.e. stroma, cytoplasm, and vacuole, or the intramembrane and intraenvelope spaces). The reaction term may in principle depend on the local value of any of the three concentrations, which we subsume into a 'vector' form $\boldsymbol{n} \equiv (n_O, n_C, n_{biC})$. The source terms are determined by flux-balance conditions to be addressed later. As all of the terms depend on the compartmental location, we introduce characteristic functions $\chi_P(r)$, $\chi_C(r)$, and $\chi_V(r)$, which are equal to one if r is respectively within the plastid, cytoplasm, or vacuole, and zero otherwise. This way, we can specify the reaction terms as

$$r_O(\boldsymbol{n}(r), r) = \chi_P(r) k_{catRO} c_R \frac{n_O(r)}{n_O(r) + n_C(r) K_{RO}/K_{RC} + K_{RO}} \tag{2}$$

$$r_C(\boldsymbol{n}(r), r) = \chi_P(r) k_{catRC} c_R \frac{n_C(r)}{n_C(r) + n_O(r) K_{RC}/K_{RO} + K_{RC}} + k_f(r) n_C(r) - k_b(r) n_{biC}(r) \tag{3}$$

$$r_{biC}(\boldsymbol{n}(r), r) = \chi_C(r) k_{catPC} c_P \frac{n_{biC}(r)}{n_{biC}(r) + K_{PC}} - k_f(r) n_C(r) + k_b(r) n_{biC}(r) \tag{4}$$

where we used stationary Michaelis-Menten forms for the competitive reaction of RuBP-primed RubisCO with O_2 and CO_2, and for the reaction of the bicarbonate with PEPC. k_f and k_b are the forward and backward reaction rates for the CO_2 to HCO_3^- interconversion. They will depend on the local pH value and on the presence or absence of the anhydrase. They are given by Johnson (1982) as[1]

$$k_f(r) = \eta_{CA}(r) \left(k_{CO_2} + k_{OH-K_w}/a_H(r) \right) \tag{5}$$

$$k_b(r) = \eta_{CA}(r) \left(k_d a_H(r) + k_{HCO_3^-} \right) \tag{6}$$

$a_H(r)$ is the proton activity, given by the local pH, $a_H = 10^{-pH}$ M, and η_{CA} is the CA-dependent reaction boost factor. It is equal one where CA is absent (e.g. vacuole), and to a large number (10^6 by default) where CA is present (i.e. in the stroma and cytoplasm). We do not allow for the CO_2-bicarbonate interconversion in the intramembrane and intraenvelope space (since it is an hydrophobic environment), so k_f and k_b are set to zero there.

---

[1]The values of the individual rates are $k_{CO_2} = 0.037\,\text{s}^{-1}$, $k_{OH-K_w} = 7.1 \cdot 10^{-11}\,\text{Ms}^{-1}$, $k_d = 7.6 \cdot 10^4\,\text{M}^{-1}\text{s}^{-1}$, and $k_{HCO_3^-} = 1.8 \cdot 10^{-4}\,\text{s}^{-1}$ (Johnson, 1982).

The source terms s_i reflect the release of O_2 and CO_2 as products of the relevant chemical pathways connected to photosynthesis. They are determined by the input the same gasses as reactants in those pathways. We first define the cumulative fluxes.

$$\Phi_{Calvin} = \int k_{catRC} c_R \frac{n_C(r)}{n_C(r) + n_O(r) K_{RC}/K_{RO} + K_{RC}} \chi_P(r) \mathrm{d}V \tag{7}$$

$$\Phi_{phresp} = \int k_{catRO} c_R \frac{n_O(r)}{n_O(r) + n_C(r) K_{RO}/K_{RC} + K_{RO}} \chi_P(r) \mathrm{d}V \tag{8}$$

$$\Phi_{C4} = \int k_{catPC} c_P \frac{n_{biC}(r)}{n_{biC}(r) + K_{PC}} \chi_C(r) \mathrm{d}V \tag{9}$$

The source terms are

$$s_O(r) = \chi_P(r) \frac{\Phi_{Calvin} + \Phi_{phresp}}{V_P} \tag{10}$$

$$s_C(r) = \chi_P(r) \frac{\Phi_{C4}}{V_P} + \chi'_C(r) \frac{\frac{1}{2}\Phi_{phresp}}{V'_C} \tag{11}$$

$$s_{biC} = 0 \tag{12}$$

where V_i stand for the volumes of particular compartments, $V_i = \int \chi_i \mathrm{d}V$. V'_C (and corresponding χ'_C) stands for the part of the peripheral cytoplasmic space accessible to the mitochondria.

The flux-balance relations incorporated in the source terms address the Hill reaction at the thylakoid (one oxygen molecule created for each CO_2 and O_2 molecule reacting with RuBP matches the NADPH creation through linear electron transfer chain with its consumption in the Calvin cycle and photorespiration), the photorespiratory CO_2 release in the mitochondria (one CO_2 molecule released for every two RuBP oxygenation events), and the release of CO_2 from the C_4 acid decarboxylation in the stroma (one CO_2 molecule for each HCO_3^- ion reacting with PEP in the cytoplasm).

The diffusion constant of a specie in a particular compartment, D_i, is equal to the diffusion constant of that specie in water $D_{i,aq}$ divided by the viscosity of the liquid filling the compartment

$$D_i(r) = D_{i,aq} \left(\frac{\chi_P(r)}{\eta_P} + \frac{\chi_C(r)}{\eta_C} + \frac{\chi_V(r)}{\eta_V} \right) \tag{13}$$

However, within the tonoplast membrane and the chloroplast envelope, the diffusion coefficient is set to reflect the permeability of the particular barrier. For a barrier with thickness θ and permeability σ_i, we'll have

$$D_i = \sigma_i \theta \tag{14}$$

Diffusion through the cell wall and plasmalemma is modelled by a boundary condition connecting the current density of CO_2 and O_2 perpendicular to the boundary surface with the difference between the local and equilibrium gas concentrations:

$$D_i \nabla n_i (r \in \partial\Omega) = \sigma_C \left(n_{i,eq} - n_i(r \in \partial\Omega) \right) \hat{e}_{\partial\Omega} \tag{15}$$

Here i stands for oxygen or carbon-dioxide (we assume the bicarbonate cannot cross the plasmalemma), $\partial\Omega$ is the cell boundary surface and $\hat{e}_{\partial\Omega}$ is the unit vector perpendicular to that surface. σ_C is the combined permeability of the cell

2

wall and the plasmalemma, while $n_{i,eq}$ is the stationary dissolved concentration of carbon-dioxide/oxygen in the thin wetting layer outside the cell wall, which is presumed to be in thermal equilibrium with the pressure of the respective gas in the internal airspace.

At other boundary surfaces we assume von Neumann boundary conditions, i.e. there is no current in or out of the simulated region

$$\nabla n_i(r \in \partial\Omega') = 0 \tag{16}$$

We have posed the model in a very general way as a system of nonlinear partial integro-differential equations in three dimensions. In reality we seize the advantage of the postulated cylindrical symmetry of the system. The resulting problem, which is effectively two-dimensional, is solved iteratively by a finite element method on a prespecified simplex mesh. The mesh is algorithmically constructed to follow the natural boundaries of the simulated system (i.e. the internal and external surface of the envelope and the tonoplast membrane). We use DUNE/PDELab libraries with BCGS solver on P_2 elements (Blatt et al., 2016; Alkämper et al., 2016). As nonlinear PDE's require iterative solving, there is a natural way to include our integrative flux-balance conditions by updating the source terms with each iteration.

The light-limited operation can be simulated by also evaluating the energy usage W^n during each iteration and scaling the concentration of RubisCO and PEPC, if the usage exceeds some capping threshold W_{cap}.

$$c_{R/P}^{n+1} = c_{R/P(\text{base})} \min\left(1, \frac{W_{cap}}{W^n}\right) \tag{17}$$

where we denoted the iteration number in the superscript. The light usage is evaluated from the overall fluxes in the energy consuming biochemical pathways.

$$W = \varphi_{Calvin}\Phi_{Calvin} + \varphi_{phresp}\Phi_{phresp} + \varphi_{C4}\Phi_{C4} \tag{18}$$

where φ_i stand for the photon cost of RuBP and PEP regeneration after each carboxylation or oxygenation event; and Φ_i are the respective fluxes.

The net carbon assimilation rate is determined by the competition of the Calvin and photorespiratory pathways:

$$A = \Phi_{Calvin} - \frac{1}{2}\Phi_{phresp} \tag{19}$$

and the net photon cost of carbon assimilation (i.e. the inverse quantum efficiency of the photosynthesis) is

$$\text{photon cost} = \frac{W}{A} \tag{20}$$

The assimilation shown in the figures is the assimilation rate per cell surface. It is obtained by dividing A with the base of the simulated cylinder

$$A_{surf} = \frac{A}{\pi r_P^2 / \phi_{P/C}} \tag{21}$$

where ϕ_{SC} is the chloroplast surface coverage.

3

References

Alkämper, M., Dedner, A., Klöfkorn, R., Nolte, M., Jan. 2016. The DUNE-ALUGrid Module. Archive of Numerical Software 4 (1), 1–28.

Blatt, M., Burchardt, A., Dedner, A., Engwer, C., Fahlke, J., Flemisch, B., Gersbacher, C., Gräser, C., Gruber, F., Grüninger, C., Kempf, D., Klöfkorn, R., Malkmus, T., Müthing, S., Nolte, M., Piatkowski, M., Sander, O., Archive Of Numerical Software, 2016. The Distributed and Unified Numerics Environment, Version 2.4. Tech. rep., University Library Heidelberg, dOI: 10.11588/ans.2016.100.26526.

Johnson, K. S., Sep. 1982. Carbon dioxide hydration and dehydration kinetics in seawater1. Limnol. Oceanogr. 27 (5), 849–855.

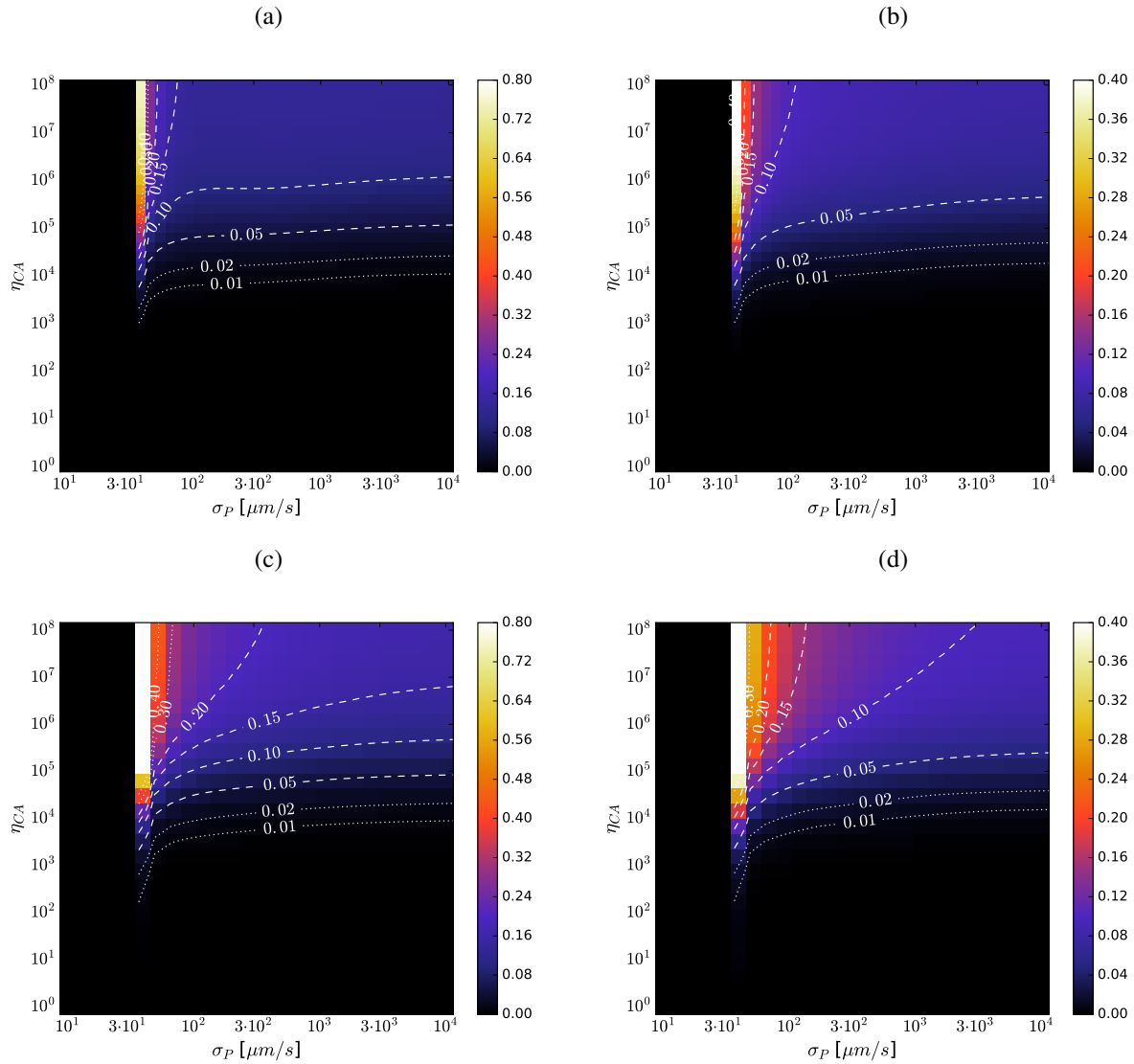# Supplementary Figures

(a)

(b)

(c)

(d)

Figure 1: CA efficacy vs. envelope permeability in C_3 photosynthesis. (a) and (b): Relative increase in carbon assimilation rate and reduction in photon cost due to presence of CA in the chloroplast stroma, as functions of the envelope permeability (σ_P) and the CO_2/HCO_3^- interconversion rate boost (η_{CA}); for $p_{CO_2} = 250\,\mu$bar and $\sigma_C = 200\,\mu$m/s. (c) and (d): Same as (a) and (b) for the case when CA is present both in the stroma and in the cytoplasm.

2
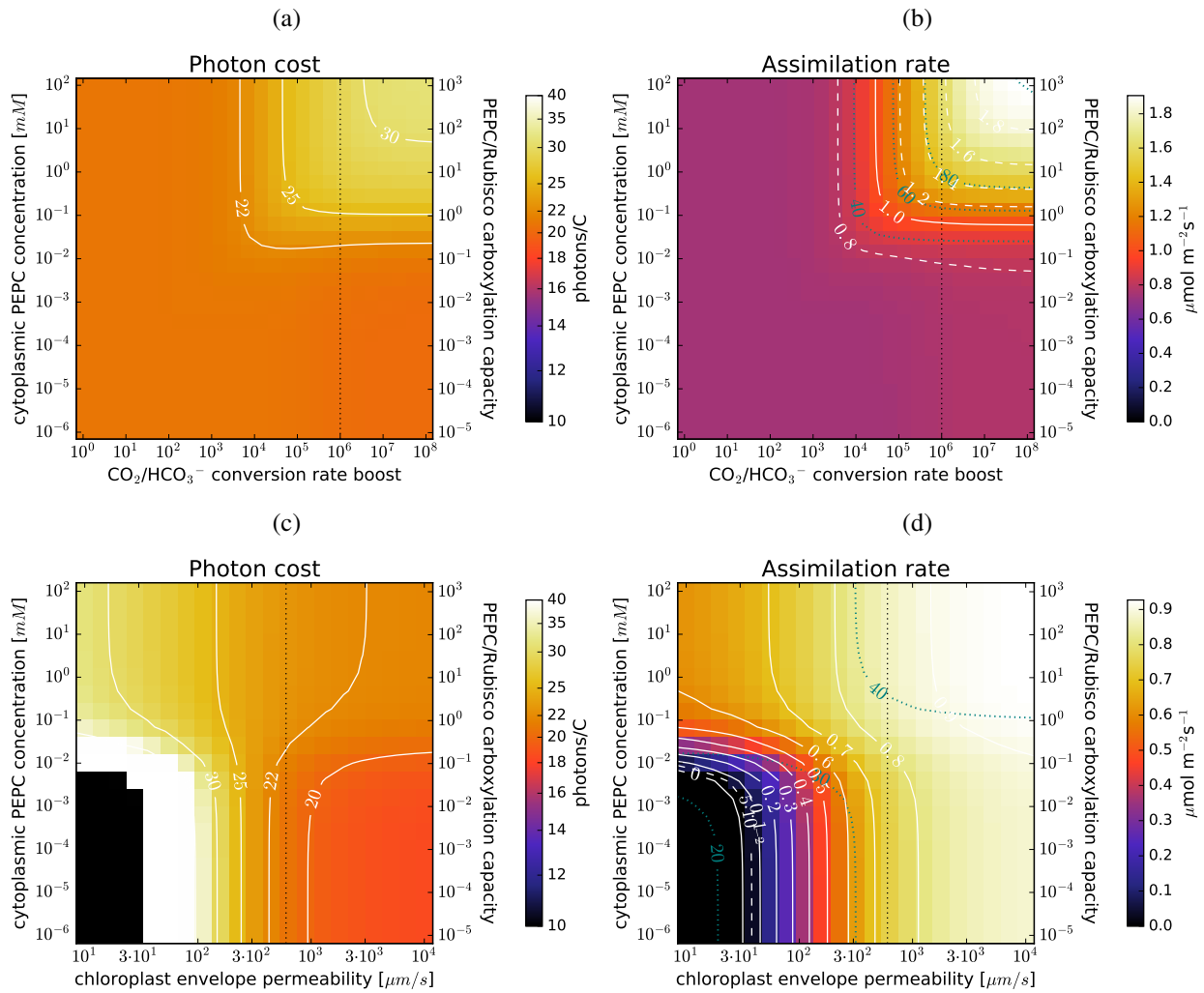
Figure 2: CA efficacy and C_4 photosynthesis: (a) and (b): the photon cost and the net assimilation rate as functions of the $CO_2 \leftrightarrow HCO_3^-$ conversion rate boost due to cytoplasmic CA (η_{CA}) and PEPC concentration in the cytoplasm (c_P), for the default parameter choice (Table 1). (c) and (d): the photon cost and the net assimilation rate as functions of the envelope permeability (σ_P) and PEPC concentration in the cytoplasm (c_P), when cytoplasmic CA is insufficient ($\eta_{CA} = 10^4$). The vertical dotted lines mark the values used as defaults in other figures.
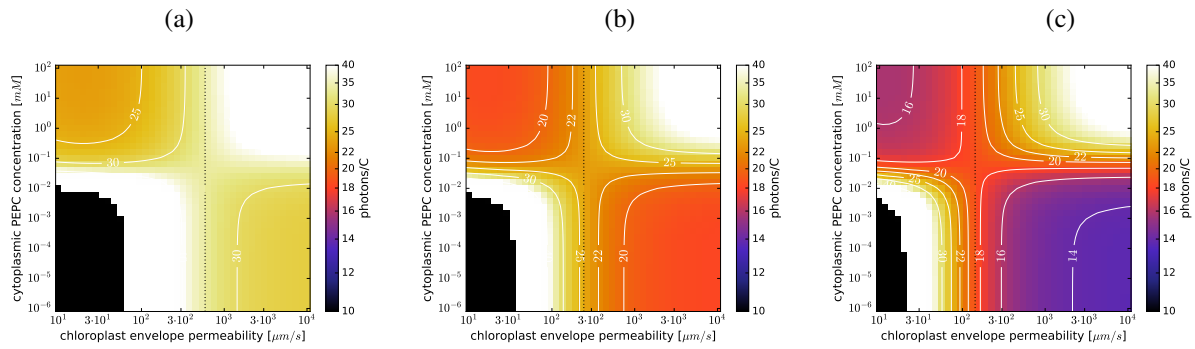
3

(a) (b) (c)

Figure 3: C_4 photosynthesis at different IAS CO_2 levels: The photon cost as a function of the envelope permeability (σ_P) and PEPC concentration in the cytoplasm (c_P) at $p_{CO_2} = 150\,\mu\text{bar}$ (a), $p_{CO_2} = 250\,\mu\text{bar}$ (b), and $p_{CO_2} = 400\,\mu\text{bar}$ (c). The dotted vertical marks the threshold envelope permeability below which the C_4 cycle is cost-efficient.
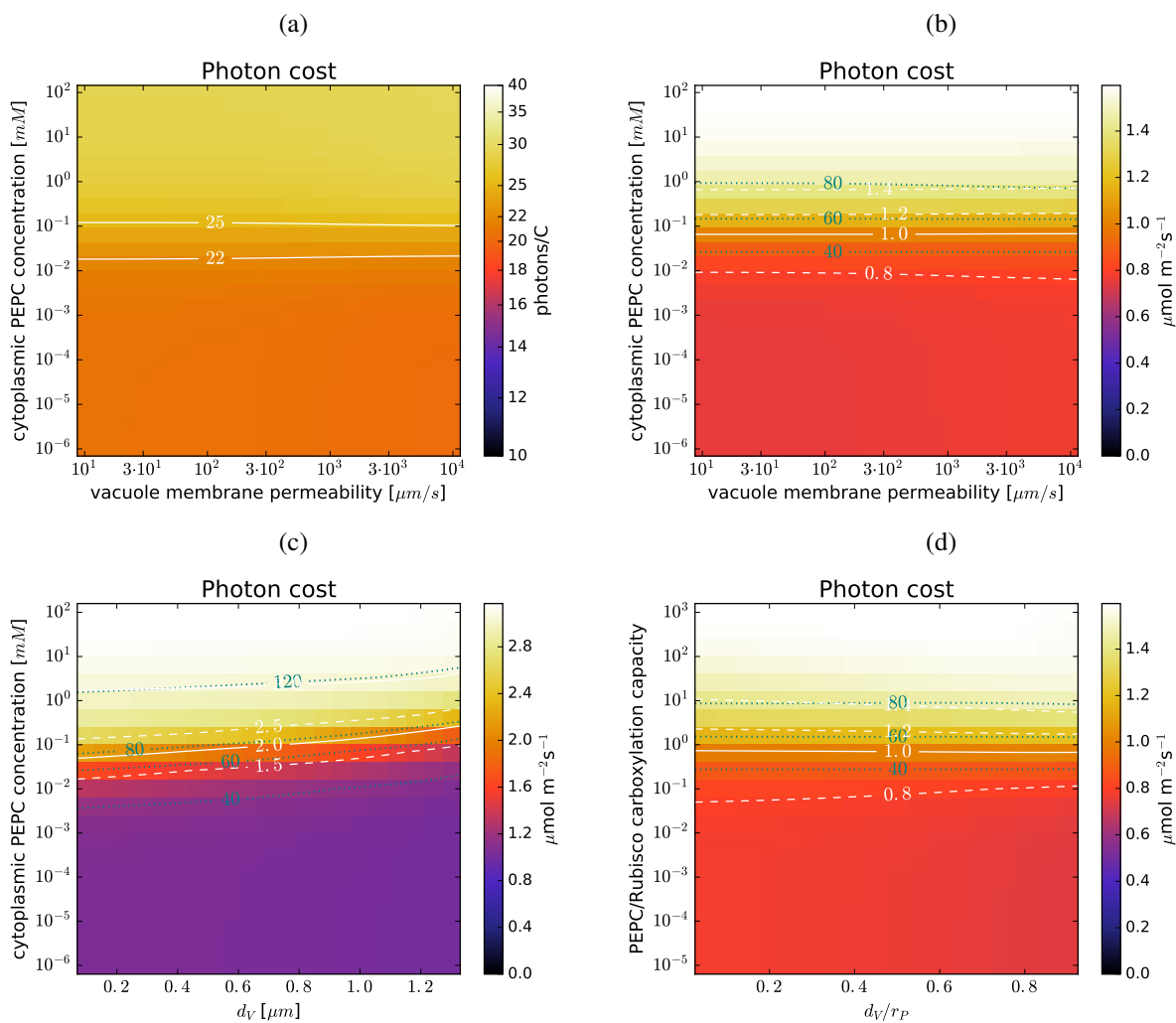
4

(a)

(b)

Photon cost

Photon cost

(c)

(d)

Photon cost

Photon cost

Figure 4: Vacuole impact on C_4 photosynthesis: (a) and (b): The photon cost and the assimilation rate as functions of the vacuole membrane permeability σ_V and the cytoplasmic PEPC level (c_P), at $\sigma_C = 200\,\mu$m/s, $\sigma_P = 600\,\mu$m/s, and $p_{CO_2} = 250\,\mu$bar. (c) and (d): The assimilation rate as a function of the drop of the vacuole (d_V) (which reduces the cytoplasmic volume) and the PEPC concentration (c) or the PEPC-to-RubisCO carboxylation capacity ratio (d). Parameters same as above, with $\sigma_V = 2\sigma_P = 1200\,\mu$m/s.
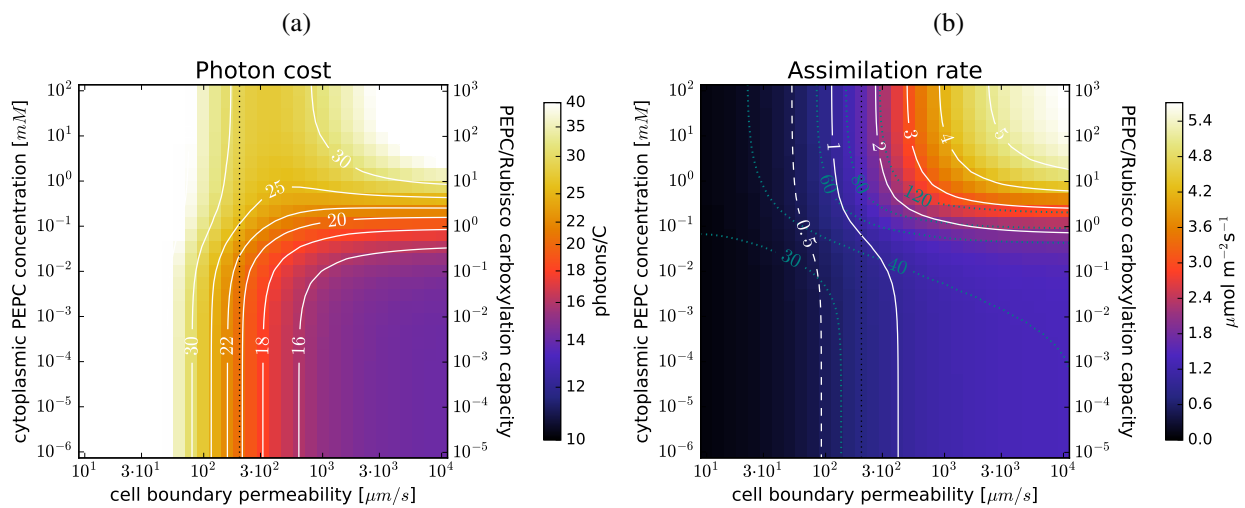
5

(a)
(b)

Figure 5: Cell wall permeability and C_4 photosynthesis: (a) and (b): the photon cost and the net assimilation rate as functions of the combined permeability of the cell wall and plsmalemma (σ_C) and PEPC concentration in the cytoplasm (c_P), for the default parameter choice (Table 1). The vertical dotted line marks the permeability used as default in other figures.

6